The International Journal of Advanced Manufacturing Technology (2022) 122:3183–3198
https://doi.org/10.1007/s00170-022-10051-3

ORIGINAL ARTICLE

Influence of dimension, building position, and orientation on mechanical properties of EBM lattice Ti6Al4V trusses

Raffaele Sepe[1] · Alessandro De Luca[2] · Venanzio Giannella[1] · Rosario Borrelli[3] · Stefania Franchitti[3] · Francesco Di Caprio[3] · Francesco Caputo[2]

Received: 30 March 2022 / Accepted: 27 August 2022 / Published online: 13 September 2022
© The Author(s) 2022

Abstract
The advent of additive manufacturing technologies significantly encouraged the development and usage of lattice structures. This paper aims to experimentally investigate the influence of dimension, building position, and orientation on the mechanical properties of Ti6Al4V trusses, manufactured by electron beam melting process, to be used in lattice cells. Specimens were manufactured considering the following parameters: truss diameter (1, 1.5, 2 mm), growth orientation (0°, 45°, 90°), and specimen position inside the building chamber. Trusses with diameter of 1 mm showed inconsistent mechanical properties caused by the poor manufacturing quality. Specimen position was found to influence the analyzed mechanical properties. Unmelted powders were observed to affect the outer surfaces of all specimens and the whole cross-sections of specimens manufactured at 0°. Specimens manufactured at 45° with diameter of 2 mm demonstrated the best performances, whereas specimens manufactured at 90° with diameter of 2 mm displayed the highest elongation at fracture.

Keywords Additive manufacturing · Electron beam melting · Lattice structures · Mechanical properties · Ti6Al4V

Abbreviations

d	Specimen diameter
E	Young's modulus
H	High level of the building chamber
L	Low level of the building chamber
θ	Building orientation
σ_{UTS}	Ultimate tensile strength
σ_{YS}	Yield stress
ε_r	Elongation at fracture
AM	Additive manufacturing
ABF	Arcam Build File
CAD	Computer-assisted design
CENT	Central area of the building plate
CORN	Corner of the building plate
EBM	Electron beam melting
PRS	Powder Recovery System
SEM	Scanning electron microscope
STL	Standard triangulation language

✉ Raffaele Sepe
rsepe@unisa.it

[1] Department of Industrial Engineering, University of Salerno, Via G. Paolo II, 132, 84084 Fisciano, Italy

[2] Department of Engineering, University of Campania "Luigi Vanvitelli", via Roma, 29, 81031 Aversa, Italy

[3] Italian Aerospace Research Centre, Structural and Material Department, CIRA, Via Maiorise, 81043 Capua, Italy

1 Introduction

A lattice structure is a space-filling unit cell that can be tessellated along any axis with no gaps between cells; hence, its architecture is formed by a collection of spatial periodic unit cells [1]. Such type of structures has been increasingly attracting the research community for the possibility to tailor their micro-architecture to match specific and multifunctional design constraints [2, 3], to design lightweight structures, as well as for their ability to provide high specific mechanical properties [4–7]. The mechanical behavior of the lattice structure can be easily changed by varying the topology of the unit cell and the size of the struts [8]. Examples of lattice structure applications are lightweight structural components, energy absorbers, and heat exchangers [9–11]. The use of lattice structures has been hindered in the past by the fact that the traditional subtractive technologies could not be used due to the several difficult and expensive cutting and welding processes mandatory for their manufacturing [12]. The advent of additive manufacturing (AM) technologies [13, 14] for metallic materials allowed designers to

manufacture components/parts that were not conceivable at all until few years ago due to the previous manufacturing limits. Lattice structures are the type of structures that have benefited the most from this innovation.

The possibility of using AM technologies [13–15] to produce complex metallic lattice structures at adequate costs increased the interest of the scientific community towards such type of structure. Several efforts have been spent to evaluate the properties of fully three-dimensional lattice structures made by AM processes [16, 17]. The advantages of the AM processes, with respect to the traditional subtractive manufacturing technologies, are numerous: increased design freedom, minimum human interaction requirement, reduced design cycle time, and limited environmental impact. Such advantages have opened a wide range of new opportunities as the possibility to topologically optimize a mechanical component for enhanced performances (e.g., weight saving) [18], the part count reduction of assemblies [19, 20], but also the possibility to manufacture components with a prescribed lattice structure micro-architecture.

To these aims, electron beam melting (EBM) is one of the most promising AM processes since it allows producing three dimensional metal parts, built layer-by-layer, starting from metal powders that are melted by a high intensity electron beam [21, 22]. During the EBM building process, a thin layer of powder is distributed, heated and selectively melted. Subsequently to the layer melting phase, according to the instructions contained in the CAD (computer-assisted design) model of the component/part to be manufactured, the building table is lowered and the sequence is repeated until the whole product is obtained. The process, firstly introduced in 1997 by the Swedish company ARCAM, is currently a promising technology for the manufacturing of lightweight, durable and dense end parts; it is mainly used in aerospace, medical and defense industries [23–26]. Similar to electron beam welding (EBW), the EBM process takes place in a vacuum chamber, providing a clean and controlled environment which avoids porosity formation inherent in many structural alloys such as Al-alloy [27, 28] as well as an excellent thermal insulation. Another unique peculiarity of EBM consists in its ability in keeping the entire build at high temperatures, above 1000 °C if needed. For each layer, the electron beam heats the entire powder bed leading the powder to an optimal temperature, specific for the used material. This ensures a good microstructure of parts free from residual stresses. It also eliminates the need of post process heat treatments, which has a significant impact on the total production costs. The high temperature process and the resulting stress-relieved components provide improved material properties better than cast and comparable to wrought [29, 30].

The EBM process can be successfully used to manufacture both massive parts, that for components having a circular cross-section it means diameter larger than 2 mm, and lattice structures, consisting basically of several truss-like elements having diameters often lower than 2 mm. Depending on the type of the structure to build, different process themes (i.e., a set of process parameters which are optimized to obtain the best results) can be used in the EBM process: the *melt* processing theme can be used to melt massive components, whereas the *net* processing theme is often used to melt lattice structures.

Titanium alloys possess excellent properties such as low density and good mechanical properties up to 550–600 °C and thus they are widely used in aerospace applications [31–33]. The development of the EBM technology in processing titanium alloys for the manufacturing of massive parts has brought the technology to an advanced state of maturity. Indeed, several studies [34–36] have been focused on the mechanical characterization of the Ti6Al4V alloy which is today one of the most promising alloys that can be processed via EBM. Further investigations on the EBM process, in terms of surface roughness, dimensional accuracy and defects distribution have been deeply faced in literature [37–41]. On the contrary, the existing literature on the EBM manufacturing of lattice structures in Ti6Al4V [42–45] is quite lack and investigations are needed to better assess their mechanical behavior and their possible use for actual structural applications. According to the existing literature, the EBM process has shown encouraging results in the manufacturing of Ti6Al4V lattice structures. However, some manufacturing imperfections, such as deviation of the real geometry from the nominal geometry defined in the CAD model as input for the process can affect negatively the performances of such lattice structures with respect to the expected ones. In particular, some researchers [29] highlighted that for thin EBM components, such as for lattice structures, both surface roughness and dimensional accuracy, which depend on the process parameters, play a crucial rule for the structural strength. With the main goal to encourage the use of lattice structures in aerospace, further studies are needed to investigate on the repeatability and the reproducibility of the process, also in terms of deviation from the expected dimensions of the product.

The mechanical characterization of AM octet truss structures should start by a well assessed approach as the building block one used for advanced aerospace structures. Figure 1 shows a scheme of such a typical approach used to mechanically characterize this type of structures.

Specifically, the first level of the proposed building block approach (the lowest one of the pyramid in Fig. 1), consists in the selection and characterization of the powders to use in the additive process; the second level consists in the mechanical characterization of the structural behavior of the single octet truss struts; the third level consists in the characterization of the elementary cell, subsequently followed by the fourth level

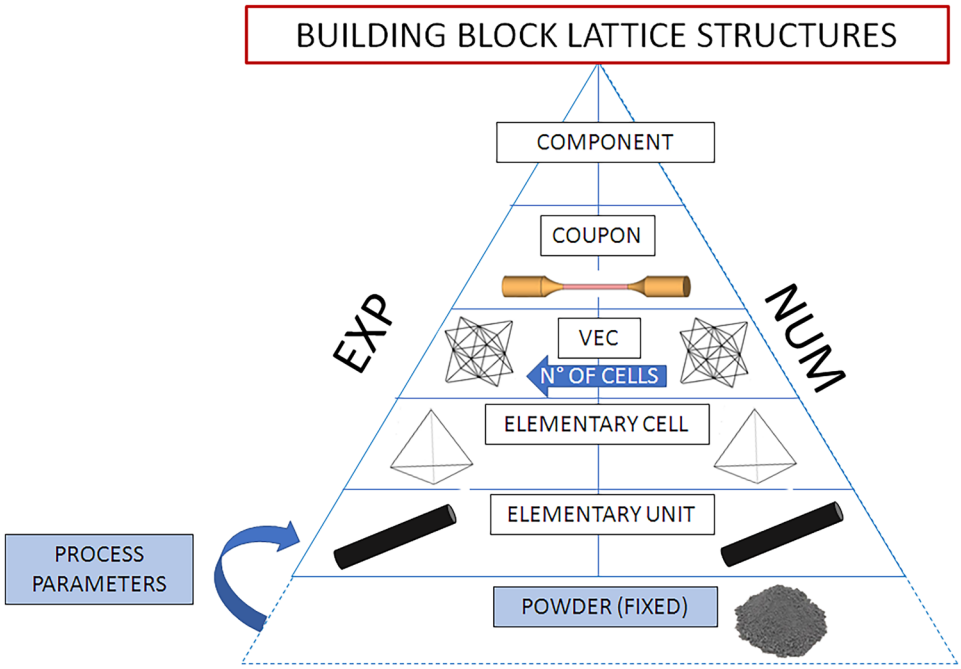

Fig. 1 AM building block approach for octet truss structures

consisting in the characterization of simple specimens made of repeated elementary cells, and finally by the characterization of the full-scale components. It has to be highlighted that the proposed approach can be supported by numerical analyses, e.g., when the experimental tests involve the unit cells, complex to be tested especially under tensile loads. This paper particularly focused on the second level, since the first one is quite established in literature, depending on manufacturing parameters and on the 3D printing technology under consideration.

The aim of this paper is to evaluate the influence of dimension, building position, and orientation on mechanical behavior of Ti6Al4V single truss-like elements made by EBM, carrying out an extensive experimental campaign on single beams representative of single truss-like elements. The experimental campaign was characterized by the usage of different nominal diameters for trusses, different growth orientations and different positions with respect to both building plate and height inside the chamber. Several Ti6Al4V samples (i.e., trusses) for tensile tests were designed and manufactured by EBM to assess the effects of such aspects on the mechanical properties.

2 Materials and methods

Ti6Al4V plasma atomized powder with spherical morphology with a nominal diameter in the range of 45 ÷ 100 µm obtained by atomization process was used to manufacture the specimens for this study. The spherical shape improves flowability and ensures high build rates and part accuracy [45]. The powder flow rate measured according to ASTM B213 [46] was found to be 24 s/50 g. The apparent density measured according to ASTM B212 [47] was 2.6 g/cm3. As regarding the particle size distribution, the percentage by mass of particle size in the range 45 ÷ 106 µm was found equal to 91%; The powder nominal chemical composition according to the ASTM F2924 [48] is reported in Table 1.

Figure 2 shows some details of a typical lattice structure based on an octet truss elementary cell. Each elementary cell can be considered the combination of two regular tetrahedra and a central body consisting of two further tetrahedra sharing the same square base. In this paper, the attention has been focused on the single trusses composing the cell, whose mechanical behavior was assessed experimentally.

To this aim, the tensile specimens adopted in this study (Fig. 3) were conceived to have the same geometry of the beam composing an octet truss structure. The gauge length of specimens presented a circular section. Three different truss diameters *d* (the nominal diameters defined as input for the process) were investigated. The length of the calibrated section was set up to 25 mm, although this parameter was not of particular interest.

The CAD software used for the drawing of the lattice structures was Solid Edge®. The geometry of the specimen

Table 1 Chemical composition of powder (wt%)

Material	Al	V	Fe	O	N	H	C	Ti
Ti6Al4V used powder [%]	6.38	4.14	0.19	0.14	0.02	< 0.003	0.01	Balance
Required [%] ASTM F2924	5.5 ÷ 6.75	3.5 ÷ 4.5	< 0.3	< 0.2	< 0.05	< 0.01	< 0.1	Balance

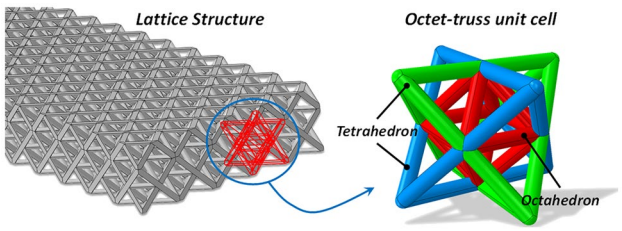

Fig. 2 Lattice structure with an octet truss cell

was modeled in two parts and two separate files were generated, one representing the specimen heads and the other one representing the gauge length, in order to assign different process themes to heads and to the gauge length. Further details are provided in the followings.

According to Fig. 4, specimens were manufactured for each of the directions defined for the beams with reference to the octet truss cell of Fig. 2. This was needed so as to quantify the influence of the truss growth directions on their mechanical behavior. Octet truss cells are expected to provide the same mechanical behavior irrespective of their position within the lattice structure. Therefore, specimens were manufactured at various locations within the building chamber (sized 210 × 210 × 380 mm × mm × mm) so as to check whether the position and the height of samples with reference to the building plate played a significant role [49]. The specimens were manufactured considering the four parameters described below:

1. Diameter: three diameters (1, 1.5 and 2 mm) were investigated;
2. Orientation (Fig. 4): three growth directions θ (0°, 45° and 90°) with respect to the building plate (x–y) were investigated. 0° direction refers to the "horizontal" orientation, whereas 90° direction refers to the "vertical" direction;
3. Location on the building plate (Fig. 4): the specimens shown in Fig. 4 were built in two different zones of the x–y building plane, named hereinafter "CENT," referring to the central position, and "CORN" referring to the corner of the plate;

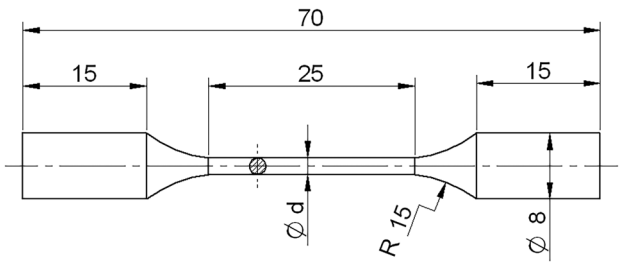

Fig. 3 Truss specimen geometry (dimensions in mm)

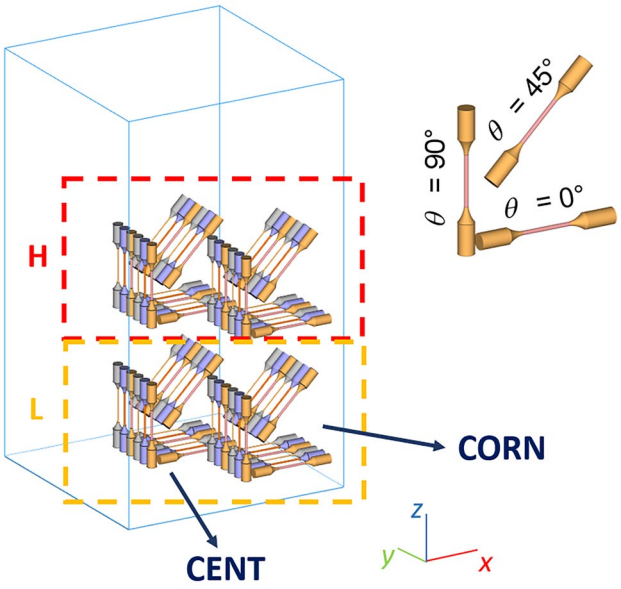

Fig. 4 Specimens manufacturing

4. Height in the building chamber (Fig. 4): specimens were built at two different heights with reference to the building plate, named hereinafter "L" and "H," referring to small (20 mm) and high (140 mm) distances from the building plate, respectively.

Considering all the possible combinations of the abovementioned 4 parameters, 36 different combinations were needed. Additionally, these combinations were replicated twice. Therefore, a total number of 72 specimens were manufactured.

2.1 EBM job preparation and specimen manufacturing

The positioning of specimens on the building platform and the generation of the supports for the specimen heads was performed by using the Magics Materialise software. Supports generation is often required by the EBM process in order to improve the heat energy dissipation and to reduce the geometric defects as curling or warping. Supports were 30 mm long and the distance between two adjacent supports was set to 3 mm.

All specimen sizes were scaled according to the ARCAM recommended scale factors (1.0092 for x and y direction and 1.0132 for z direction) so as to consider of the thermal shrinkage occurring after melting.

Afterwards, EBM Build Assembler 3.2 software was used for slicing STL (Standard Triangulation Language) files into 2D compressed layer files choosing a sliced layer thickness of 50 µm. The slicing output was the ARCAM Build File (ABF), a file containing all the information needed to perform a build in an ARCAM machine. ABF was the only file

needed to start the building process in which it was possible to view all layers and verifying layer-by-layer the building of the parts.

The process themes were defined through the EBM control 3.2 software installed on the EBM system. The automatic operating mode of the EBM system was selected and the following four standard process themes for Ti6Al4V alloy and layer thicknesses of 50 µm were used:

1. "Ti6Al4V-PreHeat-50 µm": process theme used to control the phase of preheating of the whole powder bed;
2. "Ti6Al4V-Melt-50 µm": process theme used for the realization of the specimen heads;
3. "Ti6Al4V-Net-50 µm": process theme used for the realization of the lattice part of the specimen (gauge length);
4. "Ti6Al4V-Wafer-50 µm": process theme used for the realization of the supports.

These build themes varied the EBM parameters in a controlled sequence throughout the building, according to algorithms developed by the manufacturer, in an effort to achieve parts with consistent properties. Finally, a line offset of 0.1 mm was set.

EBM system used in this investigation was the ARCAM A2X available at the Italian Aerospace Research Centre (CIRA). ARCAM A2X is designed to process titanium alloys as well as materials that require elevated temperatures such as titanium aluminide and Alloy 718. Building chamber of ARCAM A2X is specifically designed to withstand extremely high temperatures up to 1100 °C.

The EBM process by means of ARCAM A2X was carried out in a vacuum chamber. Subsequently to the job, the build was moved with a trolley directly to the Powder Recovery System (PRS) to remove and recover the sintered powder all around the melted parts (Fig. 5). Recovered powder was sieved for future use and saved in new powder containers. Once completed the PRS operation, specimens were moved to the mechanical workshop in order to remove the wafer supporting structures. The final 3D printed specimens were shown in Fig. 6. Figure 6a shows the specimens prior the removing operation, whereas Fig. 6b shows one specimen after the removing process, as mounted between the grips of the uniaxial testing machine.

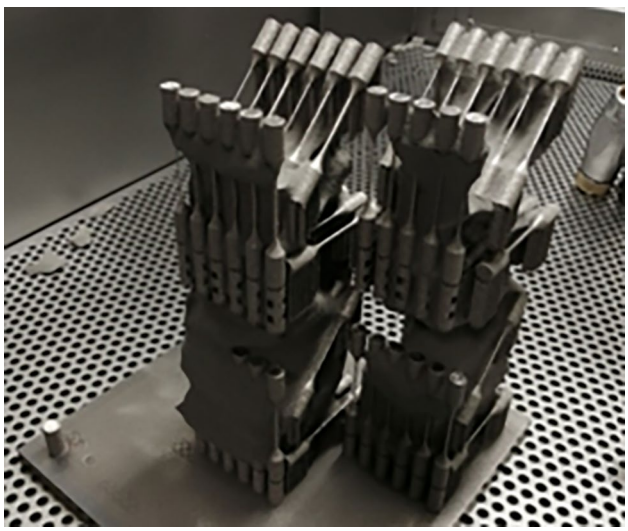

Fig. 5 Post-running operation – de-powdering of truss specimens in the PRS

2.2 Tensile tests

For the mechanical characterization of specimens, tensile tests were carried out by an MTS INSIGHT 30 electromechanical testing machine equipped with a load cell of 2 kN (Fig. 6b); strain was recorded with an MTS extensometer having a gauge length of 8 mm and a measuring range of 1.2 mm. Crosshead speed was set up to $0.26 \div 0.35$ mm/min depending on the specimen diameter.

Concerning the specimens manufactured with the $\theta = 0°$ orientation, they appeared as affected by defects as shown in Fig. 7, irrespective of all the other building parameters (i.e., location, height, and diameter). Unwanted notches were noticed nearby of all fittings between the central region and the specimen heads. As detailed in the following, these notches negatively affected the mechanical performances of all the horizontally manufactured specimens. Additionally, the horizontal manufacturing process induced consistent residual distortions to the specimens in the form of a residual bending of the specimen axis (see Fig. 7). Although it is expected that such a distortion should not play a significant role for tensile tests, much larger impact of this distortion is expected under compression (as potentially possible within a lattice structure).

In the present paper, further investigations were carried out aiming at manufacturing $\theta = 0°$ specimens without such defects, e.g., by supporting the thin specimens throughout their whole axes, gauge lengths included. Unfortunately, such defects still persisted. Results in the following referred to the first group of specimens manufactured without such supports.

3 Results and discussion

3.1 Tensile properties

This work aimed at measuring the main static mechanical properties of EBM manufactured trusses through tensile tests. Material parameters obtained by tests are Young's modulus, E; ultimate tensile strength, σ_{UTS}; yield stress, σ_{YS}; and elongation at fracture, ε_r. All stress–strain curves for each considered diameter were reported in Fig. 8. These curves were grouped

Fig. 6 Printed specimens: **a** before removing supports; **b** after removing supports; **c** installed on testing machine

by specimen growth orientation to observe that, for all considered diameters, the specimens horizontally manufactured presented a reduced mechanical resistance while, the specimens manufactured at 45° presented performances slightly higher than those ones vertically manufactured. Furthermore, specimens with larger diameters presented higher mechanical properties; indeed, all the tested samples, regardless to the diameter, have a real area of cross-section lower than their nominal area due to manufacturing imperfection. Nevertheless, the difference in percentage between the nominal area and the real area decreases as the diameter of specimen increases [29]; this means that such difference is more critical for thinner trusses. Manufacturing imperfections are due to the operating principle of the EBM process for lattice structures (net process theme). In a standard EBM melt process theme, used for massive components (having diameter/thickness greater than 2 mm), the part cross-section is melted in two stages referred to as contouring and hatching. Contouring, which is used to improve the surface finish of the part, melts the perimeter of the part cross-section. The hatching theme melts the inner part of the cross-section employing a back-and-forth raster pattern.

On the other part, the melting strategy recommended for lattice structure is based on net process theme that does not include the contouring step resulting in a more irregular cross-section. All these considerations have been deeply discussed and motivated in the following, also by observing the fracture surfaces of specimens through a scanning electron microscope (SEM).

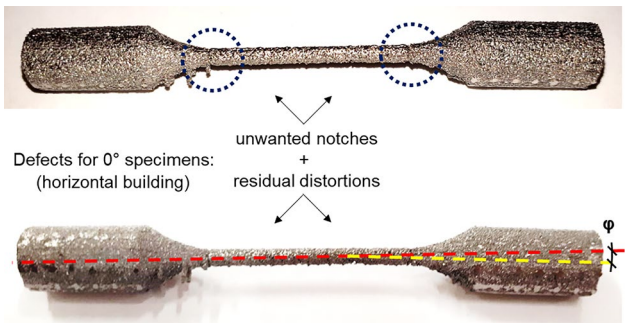

Fig. 7 Defects encountered on all specimens horizontally manufactured ($\theta = 0°$ orientation)

Main mechanical properties calculated from stress–strain curves were reported in Figs. 9, 10, 11 and 12, grouped by location/height or by growth orientation.

According to Fig. 9, some patterns were observed on Young's modulus: Young's modulus increased with the specimen diameter. This can be attributed to the fact that the reduction of the resistant cross-section is more significant in percentage for thinner diameters as stated above. Specimens manufactured in the central region of the building chamber resulted to be stiffer than those ones manufactured in the chamber corners, from 3 to 21%. This was observed for all combinations of parameters. This behavior may be explained to the fact that the different zones dissipate the heat in a different way. In particular, in the central area there are lower thermal gradients which are higher at the corners and consequently, the parts manufactured in the corners have higher residual stresses. Similar patterns were observed with reference to the height from the building plate; i.e., specimens manufactured closer to the building plate were slightly stiffer, even though this dependency seemed to be less significant. Finally, as far as the orientation is concerned, excluding the $\theta = 0°$ data (less reliable due to defects), it turned out that $\theta = 45°$ specimens resulted from 6 to 11% stiffer than $\theta = 90°$ ones depending on the specimen diameter.

Regarding the ultimate tensile strengths, σ_{UTS} (Fig. 10), and the yield stress, σ_{YS} (Fig. 11), similar observations were made: specimens manufactured centrally with respect to the building plate reported σ_{UTS} and σ_{YS} values higher than those ones manufactured at the building plate corners from 2 to 18% and from 1 to 17%, respectively. Similarly, specimens manufactured closer to the building plate were slightly more performing in terms of σ_{UTS} and σ_{YS}, even though

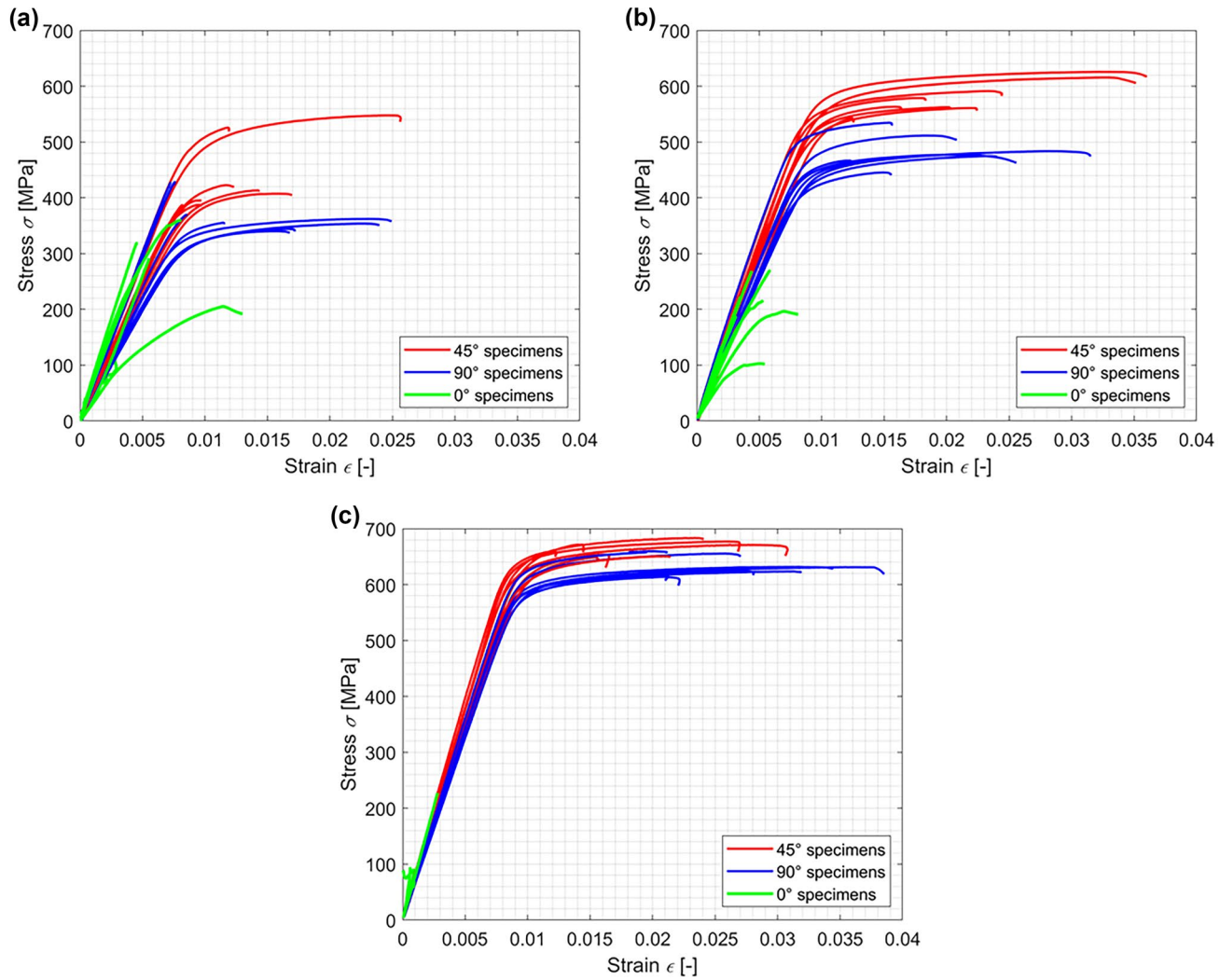

Fig. 8 Stress vs. strain curves for diameters of **a** 1 mm, **b** 1.5 mm, and **c** 2 mm

this seemed to be less relevant; σ_{UTS} of $\theta = 45°$ specimens resulted to be significantly higher ($5 \div 15\%$) than that one measured for $\theta = 90°$ specimens; increasing performances were observed as the specimen diameter increased.

Finally, with reference to the elongation at fracture, ε_r (Fig. 12), no particular tendencies were noticed.

3.2 Surface fracture analysis

Specimen failures were also analyzed to observe the failure locations along the gauge lengths. Figure 13 shows some failed specimens grouped for both growth orientation and diameter. Specifically, Fig. 13 is representative of the failure locations occurred in all tested specimens. According to the investigation, failures occurred in general at the center of the gauge length except for specimens manufactured at $\theta = 0°$. For such specimens, failures occur, on average, close to the heads this is due to the presence of notches in proximity of all fittings between the central region and the specimen heads as shown in Fig. 7. To investigate more deeply on the mechanical behavior of the tested specimens, the fracture surface of some trusses representative of the specific group classified in terms of growth orientation and diameter was observed trough SEM, as shown in Fig. 14.

According to Fig. 14, some peculiarities affecting the fracture surfaces of specimens can be observed, and linked to the specific group of specimens. As instance, looking at Fig. 14a related to the group of specimens with diameter of $d = 1$ mm and growth orientation of $\theta = 0°$, it can be noticed how the cross-section shape of trusses does not correspond to the circular section defined as input for the AM process. Indeed, Fig. 14a shows a very small fracture surface characterized by an irregular shape. Such discrepancy is more relevant for the group of specimens printed along the $\theta = 0°$ growth orientation and becomes less evident as the diameter increases. Consequently, the constitutive laws reported in

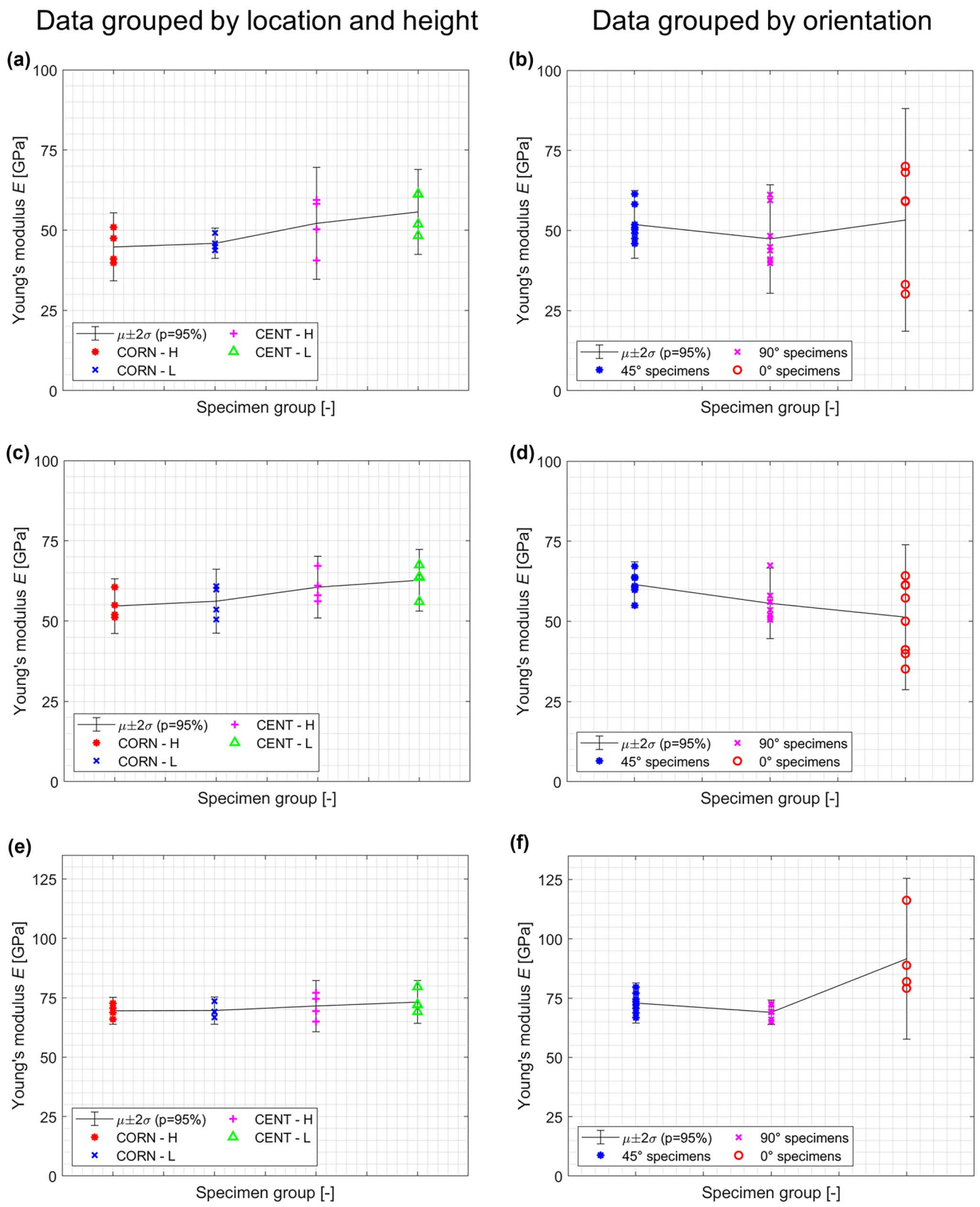

Fig. 9 Young's modulus measurements grouped by: location and height for the diameters of **a** 1 mm, **c** 1.5 mm, and **e** 2 mm; orientation for diameters of **b** 1 mm, **d** 1.5 mm, and **f** 2 mm

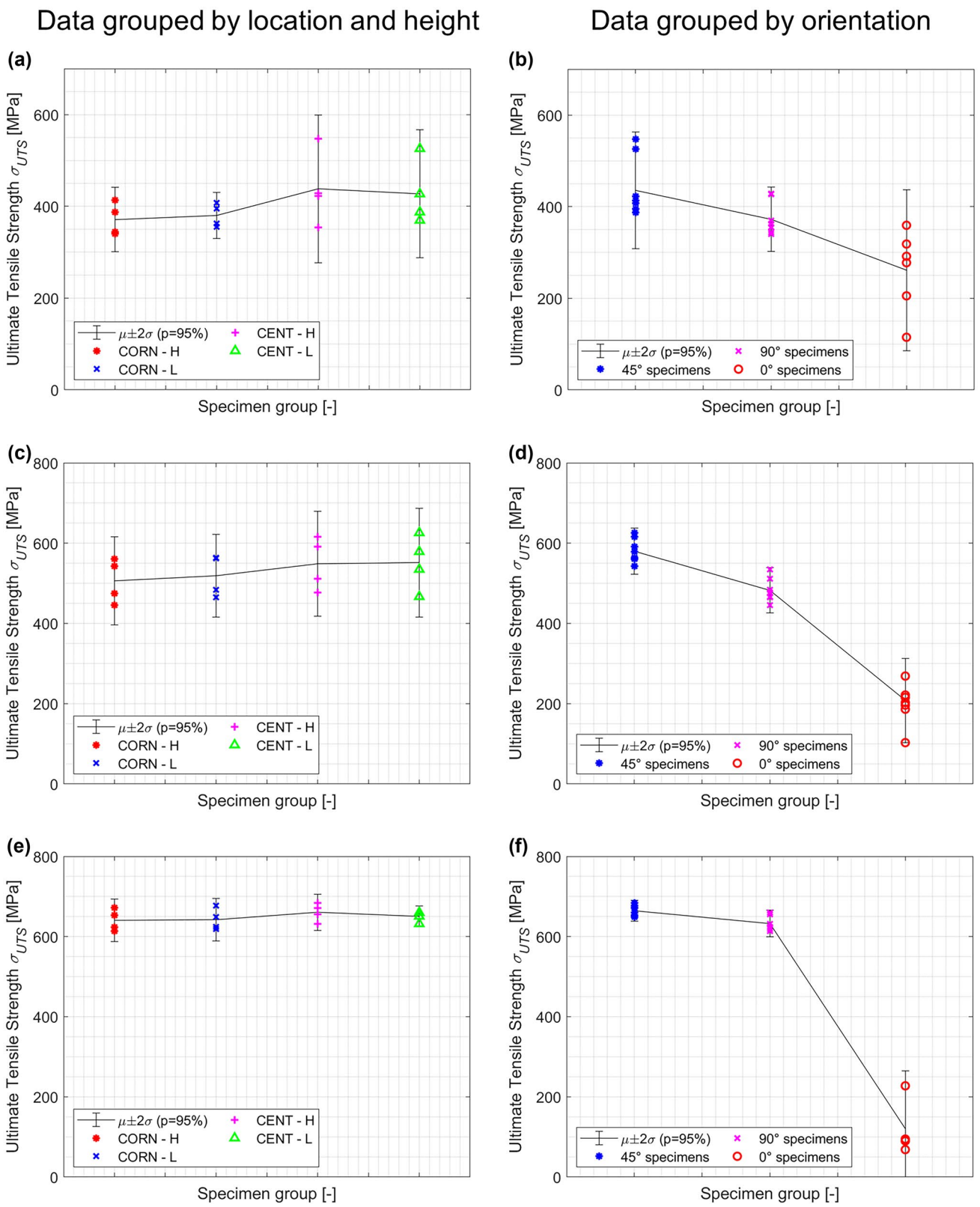

Fig. 10 Ultimate tensile strengths measurements grouped by: location and height for the diameters of **a** 1 mm, **c** 1.5 mm, and **e** 2 mm; orientation for diameters of **b** 1 mm, **d** 1.5 mm and **f** 2 mm

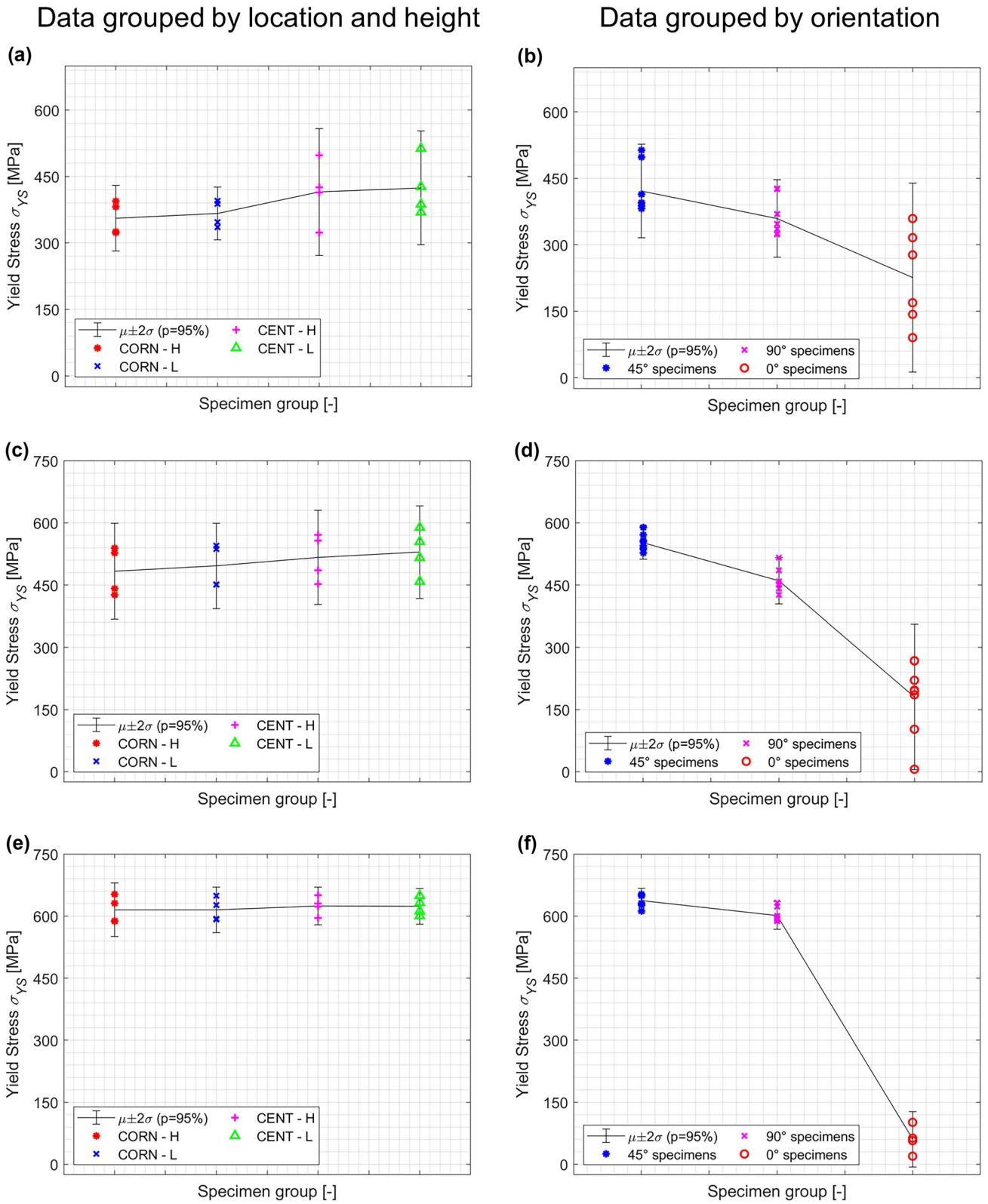

Fig. 11 Yield stress measurements grouped by: location and height for the diameters of **a** 1 mm, **c** 1.5 mm, and **e** 2 mm; orientation for diameters of **b** 1 mm, **d** 1.5 mm, and **f** 2 mm

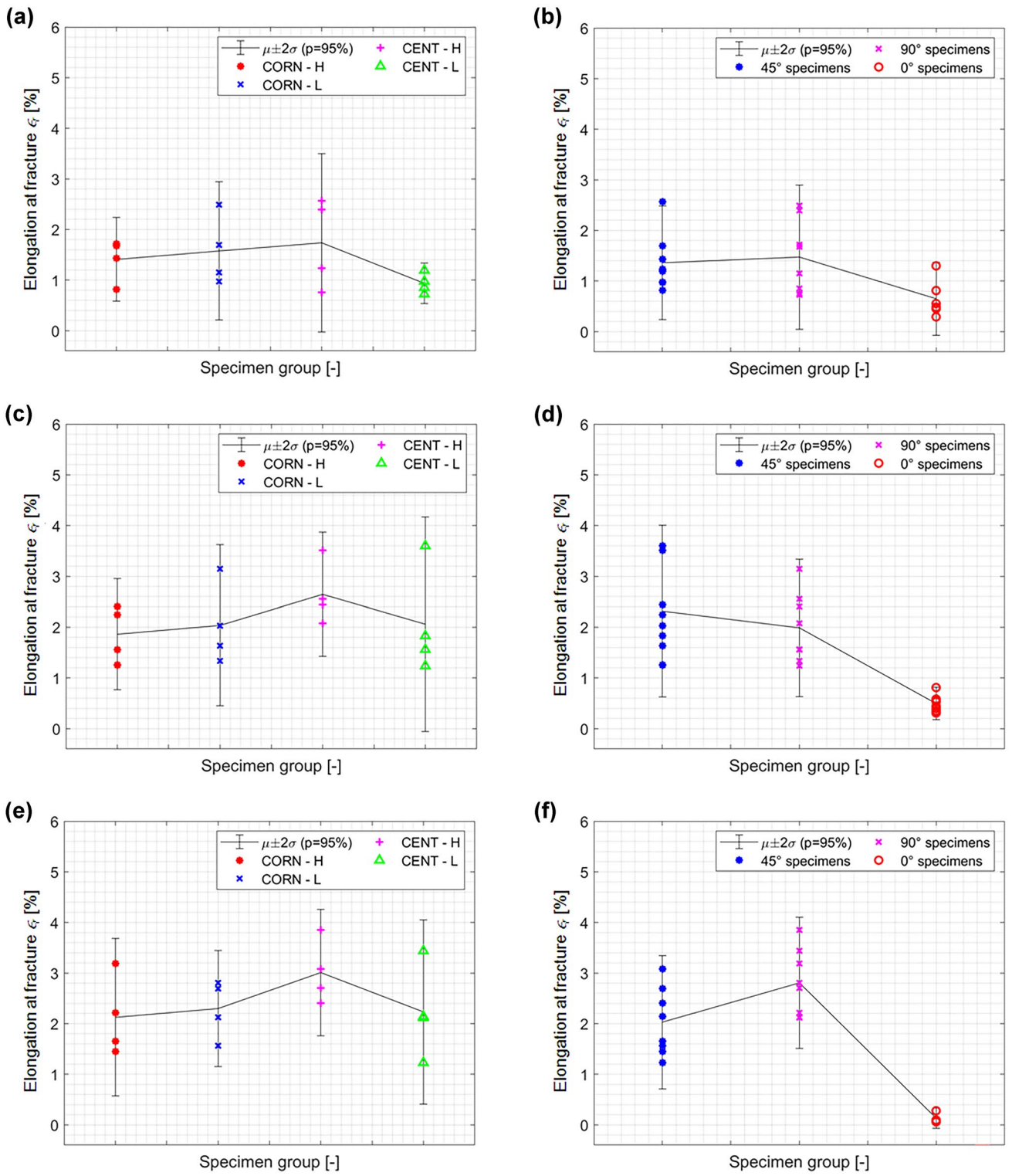

Fig. 12 Elongations at fracture measurements grouped by: location and height for the diameters of **a** 1 mm, **c** 1.5 mm, and **e** 2 mm; orientation for diameters of **b** 1 mm, **d** 1.5 mm, and **f** 2 mm

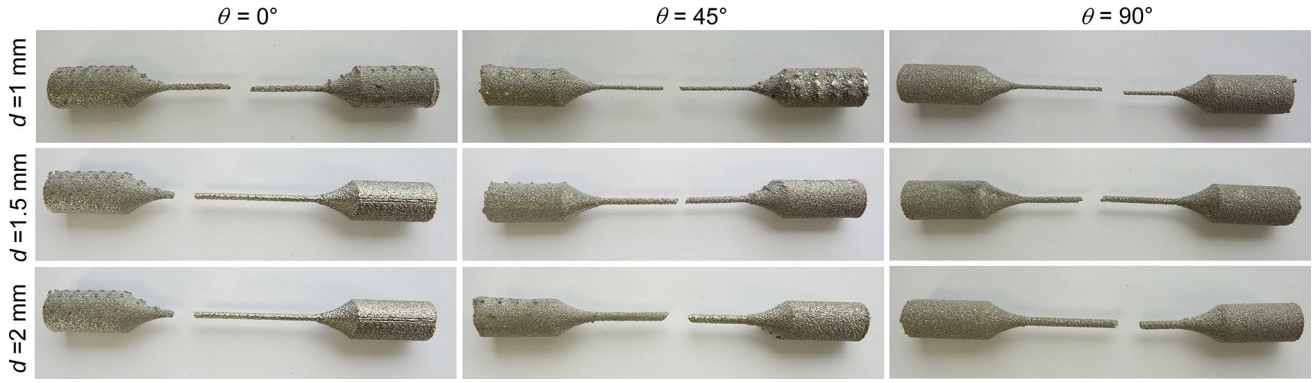

Fig. 13 Failure locations

Fig. 8a are now better motivated. Moreover, the reduced resistance can also be motivated by the fact that many defects are present in the specimens with $\theta = 0°$: there are large cavities (Fig. 14b) due to lack of fusion between the deposition layers, and unmelted powders (Fig. 14c). Therefore, these defects play a principal role in the fracture of the specimens with $\theta = 0°$ when these are subjected to uniaxial tensile load. In Fig. 15a at a large magnification, dimples and cleavage facets can be observed on the fracture surfaces indicating ductile and brittle mixed mode fracture behavior.

Comparing such group of specimens with those ones obtained at different growth orientations ($\theta = 45°$ and 90°), it can be noticed that for the latter, a lower quantity of defects affects the specimens. The cross-sections, apart from the outer contour, was found to be more well melted showing very few voids (red circled in Fig. 14) and small zones with unmelted powders (Fig. 14d–i). Also, the shape, in these two groups of specimens, appeared to be closer to the expected circular one defined in the CAD model. According to the fracture surface shown in Fig. 14f, it can be observed that the group of specimens with growth orientation of $\theta = 45°$ and diameter of $d = 2$ mm was very well printed, in terms of shape and size. This resulted in an evident correspondence with the structural response of such group of specimens, represented by the constitutive laws reported in Fig. 8c. As matter of the fact, specimens with diameter of $d = 2$ mm and growth orientation of $\theta = 45°$ demonstrated a higher resistance with respect to the others.

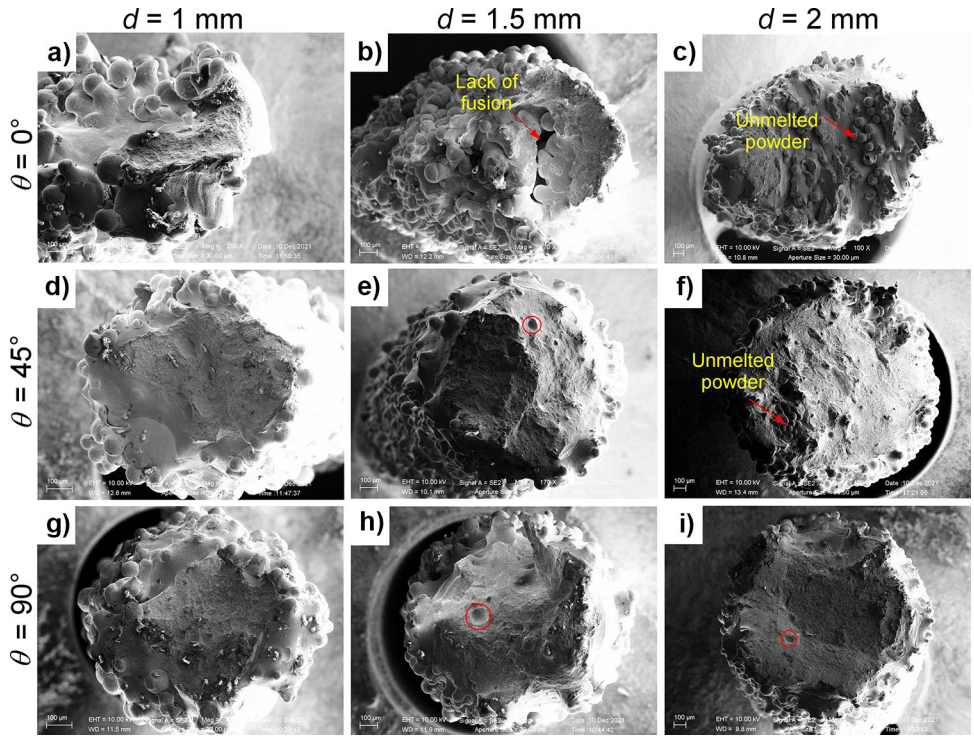

Fig. 14 Fracture surfaces of specimens at SEM

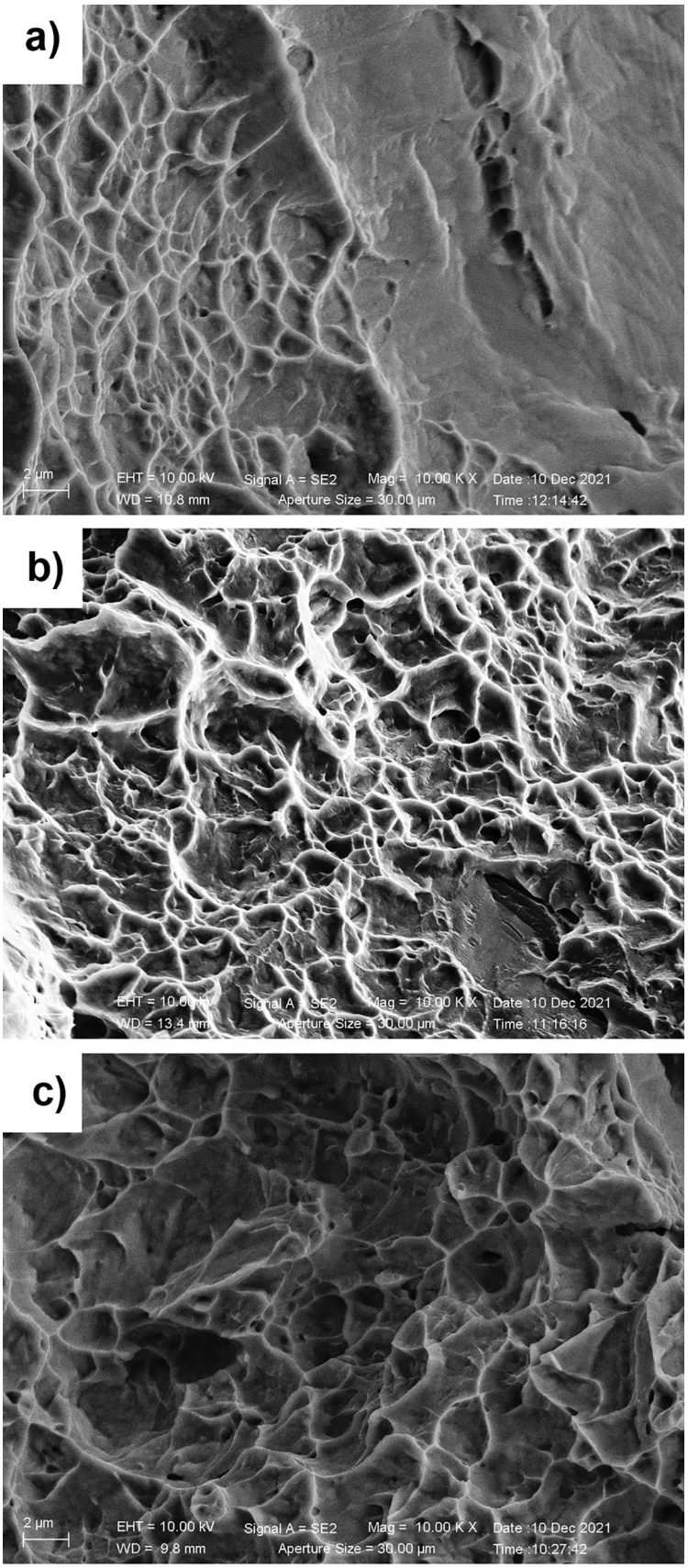

Fig. 15 Details of fracture surfaces at SEM for specimens with $d=2$ mm: **a** $\theta=0°$; **b** $\theta=45°$; **c** $\theta=90°$

Furthermore, Fig. 15b shows a ductile fracture surface with presence of a large number of fine dimples that indicate a good ductility. The fracture mode of specimens with $\theta = 90°$ (Fig. 15c) was found to be similar to $\theta = 45°$ specimens (Fig. 15b), except for the higher quantity of micro-voids.

4 Conclusions

This paper aims to investigate on the mechanical behavior of the single octet truss struts composing the lattice unit cell, as the octet-truss ones, according to the building block approach herein proposed to characterize such type of engineering structures.

This paper focused the attention on the mechanical characterization of single Ti-6Al-4 V struts composing an elementary octet truss cell, printed through EBM technology. For this purpose, several tensile tests were carried out by changing some relevant parameters, such as struts diameter, growth orientation, in-plane position on the building plate, and height in the building chamber. The main mechanical properties of each specimen group were derived from test data to arrange a discussion in terms of stress–strain curves, Young's modulus, ultimate tensile strength, yield stress, and elongation at fracture.

According to these test results, it was observed that the horizontally manufactured specimens presented a very reduced mechanical resistance as well as a more brittle behavior. In all specimens manufactured at $\theta = 0°$, unmelted powders were observed to affect the outer surfaces of all specimens and the whole cross-sections. Moreover, for such group of specimens, it was found that the cross-section shape did not correspond to the circular section defined as input for the AM process. Cross-section of $d = 1$ mm specimens resulted very small and characterized by irregular profiles. Such aspect became less evident as the diameter increased, nonetheless still present. In general, the larger the diameter was, the higher the resistance of specimens resulted to be. This was attributed to the fact that when specimens with small diameters were built, large discrepancies were obtained between the nominal and the actual specimen cross-section area. Finally, incomplete melting of powder was observed at the outer surface of the specimens for all the other growing directions.

With respect to the specimen dimensions, increasing performances were observed as the specimen diameter increased. Concerning the specimen location, specimens manufactured at the central region of the building chamber and closer to the building plate resulted to be stiffer than the others. Centrally manufactured specimens, with respect to the building plate, reported σ_{UTS} and σ_{YS} values higher than those ones manufactured at the building plate corners. Similarly, specimens manufactured closer to the building plate were slightly more performant in terms of σ_{UTS} and σ_{YS}, even though this tendency seemed to be less significant.

Concerning the specimen orientations and excluding the $\theta = 0°$ data (less reliable due to defects), $\theta = 45°$ specimens appeared stiffer than 90° ones, presenting performances slightly higher than those ones vertically manufactured. σ_{UTS} of 45° specimens was found to be higher than that one measured for $\theta = 90°$ specimens.

Author contribution R. Sepe conceived and designed the analysis, carried out the experimental tests, performed the analysis, and wrote the paper. V. Giannella carried out the experimental tests, collected the data, performed the analysis, and wrote the paper. A. De Luca conceived and designed the analysis, collected the data, and wrote the paper. R. Borrelli conceived and designed the analysis, and supervised the analysis. S. Franchitti conceived and designed the analysis, and manufactured the specimens. F. Di Caprio conceived and designed the analysis, wrote the paper, and supervised the analysis. F. Caputo conceived and designed the analysis, and supervised the analysis.

Funding Open access funding provided by Università degli Studi di Salerno within the CRUI-CARE Agreement.

Data availability Data and materials are presented in the manuscript.

Declarations

Ethical approval and consent to participate Not applicable.

Consent for publication The authors declare that this work has not been published before, that it is not under consideration for publication elsewhere, that its publication has been approved by all coauthors, and that its publication has been approved by the responsible authorities at the institution where the work is carried out.

Competing interests The authors declare no competing interests.

Open Access This article is licensed under a Creative Commons Attribution 4.0 International License, which permits use, sharing, adaptation, distribution and reproduction in any medium or format, as long as you give appropriate credit to the original author(s) and the source, provide a link to the Creative Commons licence, and indicate if changes were made. The images or other third party material in this article are included in the article's Creative Commons licence, unless indicated otherwise in a credit line to the material. If material is not included in the article's Creative Commons licence and your intended use is not permitted by statutory regulation or exceeds the permitted use, you will need to obtain permission directly from the copyright holder. To view a copy of this licence, visit http://creativecommons.org/licenses/by/4.0/.

References

1. Helou M, Kara S (2018) Design, analysis and manufacturing of lattice structures: an overview. Int J Comp Integ M 31(3):243–261
2. Berger JB, Wadley HNG, McMeeking RM (2017) Mechanical metamaterials at the theoretical limit of isotropic elastic stiffness. Nature 543(7646):533–537

3. Zheng X, Lee H, Weisgraber TH, Shusteff M, DeOtte J, Duoss EB et al (2014) Ultralight, ultrastiff mechanical metamaterials. Science 344(6190):1373–1377
4. Fleck NA, Deshpande VS, Ashby MF (2010) Micro-architectured materials: past, present and future. Proc R Soc London Math Phys Eng Sci 466(2121):2495–2516
5. Ashby M (2011) Hybrid materials to expand the boundaries of material-property space. J Am Ceram Soc 94:3–14
6. Ashby MF (2005) Materials selection in mechanical design, 3rd edition. Elsevier Press.
7. Ferrigno A, Di Caprio F, Borrelli R, Auricchio F, Vigliotti A (2019) The mechanical strength of Ti-6Al-4V columns with regular octet microstructure manufactured by electron beam melting. Materialia 5:100232
8. Pan C, Han Y, Lu J (2020) Design and optimization of lattice structures: a review. Appl Sci 10(18):6374
9. Al-Ketan O, Abu Al-Rub RK (2019) Multifunctional mechanical metamaterials based on triply periodic minimal surface lattices. Adv Eng Mat 21(10):1900524
10. Choy SY, Sun CN, Sin WJ, Leong KF, Su PC, Wei J et al (2021) Superior energy absorption of continuously graded microlattices by electron beam additive manufacturing. Virtual Phys Prototyp 16(1):1–15
11. Maconachie T, Leary M, Lozanovski B, Zhang X, Qian M, Faruque O et al (2019) SLM lattice structures: properties, performance, applications and challenges. Mater Design 183:108137
12. Kooistra GW, Deshpande VS, Wadley HNG (2004) Acta Mater 52:4229
13. Zhang Y, Wu L, Guo X, Kane S, Deng Y, Junget YG et al (2018) Additive manufacturing of metallic materials: a review. J of Materi Eng and Perform 27:1
14. Çam G (2022) Prospects of producing aluminum parts by wire arc additive manufacturing (WAAM). Mater Today Proc. https://doi.org/10.1016/j.matpr.2022.02.137
15. Citarella R, Giannella V (2021) Additive manufacturing in industry. Appl Sci 11(2):840
16. Parthasarathy J, Starly B, Raman S, Christensen A (2010) Mechanical evaluation of porous titanium (Ti-6Al-4V) structures with electron beam melting (EBM). J Mech Behav Biomed 3(3):249–259
17. Carlton HD, Lind J, Messner MC, Volkoff-Shoemaker NA, Barnard HS, Barton NR et al (2017) Mapping local deformation behavior in single cell metal lattice structures. Acta Mater 129:239–250
18. Armentani E, Giannella V, Parente A, Pirelli M (2020) Design for NVH: topology optimization of an engine bracket support. Procedia Struct Integr 26:211–218
19. Shapiro AA, Borgonia JP, Chen QN, Dillon RP, McEnerney B, Polit-Casillas R et al (2016) Additive manufacturing for aerospace flight applications. J Spacecraft Rockets 53(5):952–959
20. Sepe R, Giannella V, Alfieri V, Caiazzo F (2021) Static and fatigue behavior of laser welded additively manufactured 17–4 PH steel plates. Procedia Struct Integr 34:172–177
21. Körner C (2016) Additive manufacturing of metallic components by selective electron beam melting-a review. Int Mater Rev 61(5):361–377
22. Gong X, Anderson T, Chou K (2014) Review on powder-based electron beam additive manufacturing technology. Manuf Rev 1:1–12
23. Li MX, Qu WQ (2014) Electron beam additive manufacturing and its applications in aerospace field. Mater Sci Forum 789:377–383
24. Tan X, Kok Y, Tor SB, Chua CK (2014) Application of electron beam melting (EBM) in additive manufacturing of an impeller. Proc Int Conf Prog Addit Manuf (Pro-AM 2014) 327–332
25. Murr LE, Quinones SA, Gaytan SM, Lopez MI, Rodela A, Martinez EY et al (2009) Microstructure and mechanical behavior of Ti–6Al–4V produced by rapid-layer manufacturing, for biomedical applications. J Mech Behav Biomed 2(1):20–32
26. Zhao S, Hou WT, Xu QS, Li SJ, Hao YL, Yang R (2018) 3.5 - Ti-6Al-4V lattice structures fabricated by electron beam melting for biomedical applications. In Froes FH, Qian M, eds. Proceeding of Woodhead Publishing Series in Biomaterials, Titanium in Medical and Dental Applications. Woodhead Publishing 277–301
27. Çam G, Ventzke V, dos Santos JF, Koçak M, Jennequin G, Gonthier-Maurin P (1999) Characterisation of electron beam welded aluminium alloys. Sci Technol Weld Join 4(5):317–323
28. Çam G, Koçak M (2007) Microstructural and mechanical characterization of electron beam welded Al-alloy 7020. J Mater Sci 42(17):7154–7161
29. Sepe R, Franchitti S, Borrelli R, Di Caprio F, Armentani E, Caputo F (2020) Correlation between real geometry and tensile mechanical behaviour for Ti6Al4V Electron Beam Melted thin specimens. Theor Appl Fract Mech 102519
30. Murr LE, Esquivel EV, Quinones SA, Gaytan SM, Lopez MI, Martinez EY et al (2009) Microstructures and mechanical properties of electron beam-rapid manufactured Ti–6Al–4V biomedical prototypes compared to wrought Ti–6Al–4V. Mater Charact 60(2):96–105
31. Cam G, Flower HM, West DRF (1991) Constitution of Ti-Al-C alloys in the temperature range 1250–750 °C'. Mater Sci Tech 7(6):505–511
32. Çam G, Clemens H, Gerling R, Koçak M (1999) Diffusion bonding of fine grained gamma-TiAl sheets. Z Metallkd 90(4):284–288
33. Çam G, dos Santos JF, Koçak M (1997) Laser and electron beam weldability of Ti-alloys: literature review. GKSS 97/E/35, GKSS Research Center, Geesthacht, Germany, IIW Doc IX-1897–98
34. Facchini L, Magalini E, Robotti P, Molinari A (2009) Microstructure and mechanical properties of Ti-6Al-4V produced by electron beam melting of pre-alloyed powders. Rapid Prototyp J 15(3):171–178
35. Pirozzi C, Franchitti S, Borrelli R, Caiazzo F, Alfieri V, Argenio P (2017) Study on the factors affecting the mechanical behavior of electron beam melted Ti-6Al-4V. J Mater Eng Perform 26(9):4491–4499
36. Mohammadhosseini A, Fraser D, Masood SH, Jahedi M (2013) Microstructure and mechanical properties of Ti-6Al-4V manufactured by electron beam melting process. Mater Res Innov 17(2):106–112
37. Chern AH, Nandwana P, Mcdaniels R, Dehoff RR, Liaw PK, Tryon R et al (2020) Build orientation, surface roughness, and scan path influence on the microstructure, mechanical properties, and flexural fatigue behavior of Ti–6Al–4V fabricated by electron beam melting. Mater Sci Eng A 772
38. Borrelli R, Franchitti S, Pirozzi S, Carrino L, Nele L, Polini W et al (2020) Ti-6Al-4V parts produced by electron beam melting: analysis of dimensional accuracy and surface roughness. J Adv Manuf Technol 19(1):1–24
39. Franchitti S, Borrelli R, Pirozzi C, Carrino L, Polini W, Sorrentino L et al (2018) Investigation on electron beam melting: dimensional accuracy and process repeatability. Vacuum 157:340–348
40. Pirozzi C, Franchitti S, Borrelli R, Diodati G, Vatasso G (2019) Experimental study on the porosity of electron beam melting-manufactured Ti-6Al-4V. J Mater Eng Perform 28(5):2649–2660
41. Franchitti S, Pirozzi C, Borrelli R (2020) Influence of hot isostatic pressing and surface finish on the mechanical behaviour of Ti-6Al-4V processed by electron beam melting. Fatigue Fract Eng Mater Struct 1–14

42. Van Grunsven W, Hernandez-Nava E, Reilly GC, Goodall R (2014) Fabrication and mechanical characterisation of titanium lattices with graded porosity. Metals 4:401–409
43. Xiao L, Song W, Wang C, Liu H, Tang H, Wang J (2015) Mechanical behavior of open-cell rhombic dodecahedron Ti–6Al–4V lattice structure. Mater Sci Eng A 640:375–384
44. Li SJ, Murr LE, Cheng XY, Zhang ZB, Hao YL, Yang R et al (2012) Compression fatigue behavior of Ti–6Al–4V mesh arrays fabricated by electron beam melting. Acta Mater 60(3):793–802
45. Del Guercio G, Galati M, Saboori A, Fino P, Iuliano L (2020) Microstructure and mechanical performance of Ti–6Al–4V lattice structures manufactured via electron beam melting (EBM): a review. Acta Metall Sin (Engl Lett) 33:183–203
46. ASTM Standard B213 (2020) Standard Test Methods for Flow Rate of Metal Powders Using the Hall Flowmeter Funnel, ASTM International, West Conshohocken, PA, 2020
47. ASTM Standard B212 (2021) Standard Test Method for Apparent Density of Free-Flowing Metal Powders Using the Hall Flowmeter Funnel, ASTM International, West Conshohocken, PA, 2021
48. ASTM Standard F2924 (2021) Standard Specification for Additive Manufacturing Titanium-6 Aluminum-4 Vanadium with Powder Bed Fusion, ASTM International, West Conshohocken, PA, 2021
49. Alfieri V, Giannella V, Caiazzo F, Sepe R (2022) Influence of position and building orientation on the static properties of LPBF specimens in 17–4 PH stainless steel. Forces Mech 8:100108

Publisher's note Springer Nature remains neutral with regard to jurisdictional claims in published maps and institutional affiliations.